Geochemistry Geophysics Geosystems G3
AN ELECTRONIC JOURNAL OF THE EARTH SCIENCES
Published by AGU and the Geochemical Society

Article
Volume 3, Number 11
6 November 2002
8603, doi:10.1029/2001GC000289
ISSN: 1525-2027

Dunite distribution in the Oman Ophiolite: Implications for melt flux through porous dunite conduits

Michael G. Braun and Peter B. Kelemen

Department of Marine Geology and Geophysics, Woods Hole Oceanographic Institution, Woods Hole, Massachusetts, USA (mbraun@whoi.edu; peterk@whoi.edu)

[1] Dunites in the mantle section of the Oman ophiolite represent conduits for chemically isolated melt transport through the shallow mantle beneath oceanic spreading centers. These dunite melt conduits exhibit a scale-invariant power law relationship between width and cumulative abundance, as measured over 4 orders of magnitude. We use this size/frequency distribution to assess several hypotheses for dunite formation and estimate the total melt flux that a dunite network can accommodate beneath an oceanic spreading center. Dunites, measured from one-dimensional lithologic sections and digital image mosaics at a variety of length scales, range in width from ~3 mm to ~100 m and follow a power law with a slope of ~1.1. Extrapolation of the power law predicts that dunites as wide as 3.5 km may exist in the melting region beneath a mid-ocean ridge. Alternatively, perhaps the widest dunites we observe (~100 m) represent a maximum size. Modeling of dunites as diffusive reaction zones around melt-filled hydrofractures cannot explain the existence of dunites wider than ~10 m in Oman. Instead, dunites may represent high porosity conduits formed by reactive porous flow. Using the observed size/frequency relationship, the assumption that dunites form a coalescing network and the requirement that flux is conserved where dunites merge, we estimate the total flux through a porous dunite network and the fraction of that flux that remains chemically isolated. Our flux model predicts that the porosity in a dunite scales with the width. For maximum porosities of ~1–4% in the widest dunites, a network of porous dunite conduits with the abundances observed in Oman can supply a sufficient flux of melt (of which > 95% remains chemically unequilibrated with shallow residual peridotites) to satisfy the observed mid-ocean ridge flux.

Components: 9654 words, 16 figures, 1 table.

Keywords: Dunites; melt migration/extraction; Oman ophiolite; mid-ocean ridges.

Index Terms: 3035 Marine Geology and Geophysics: Midocean ridge processes; 3250 Mathematical Geophysics: Fractals and multifractals; 5114 Physical Properties of Rocks: Permeability and porosity; 8434 Volcanology: Magma migration.

Received 4 December 2001; **Revised** 6 May 2002; **Accepted** 10 May 2002; **Published** 6 November 2002.

Braun, M. G., and P. B. Keleman, Dunite distribution in the Oman Ophiolite: Implications for melt flux through porous dunite conduits, *Geochem. Geophys. Geosyst.*, *3*(11), 8603, doi:10.1029/2001GC000289, 2002.

Theme: The Oman Ophiolite and Mid-Ocean Ridge Processes
Guest Editors: Peter Kelemen, Chris Macleod, and Susumu Umino

1. Introduction

[2] Geophysical and geochemical observations suggest that melt transport beneath oceanic spreading centers is strongly focused toward the ridge axis and rapidly extracted from the shallow mantle predominantly via chemically isolating dunite conduits. In this study we examine the abundance and size distribution of dunite conduits preserved in the Oman Ophiolite to assess proposed mechanisms of dunite formation and place constraints on the melt flux that the dunite network can accommodate.

[3] Recent geophysical data indicate that the melting region beneath mid-ocean ridges is much larger than the seismically determined zone of crustal accretion at the ridge axis. Seismic data from the MELT experiment (17°S along the East Pacific Rise) indicate that melt is present for several hundred kilometers off-axis and to depths of 120–150 km [*Forsyth et al.*, 1998]. However, seismic velocity data indicate the igneous oceanic crust attains its complete thickness within 5 km of the ridge axis [*Dunn et al.*, 2000; *Vera et al.*, 1990]. Geochemical studies show that lateral melt migration from a broad region of corner flow is required to reproduce the trace element characteristics of MORB [*Spiegelman*, 1996]. Therefore melts must be efficiently extracted from a broad melting region and transported to the ridge axis to be accreted within the narrow ridge axis. Although our understanding of the exact path of melt migration through the upper mantle is incomplete, several geochemical and morphological constraints can be placed on the nature of the melt transport system.

[4] Since mid-ocean ridge basalt (MORB) is not in chemical equilibrium with residual harzburgite in the shallow mantle, melt extraction must occur in chemically isolated conduits. Primitive MORBs are undersaturated in orthopyroxene (opx) with respect to the equilibrium cotectic melt composition at pressures commensurate with the base of the oceanic crust (1–2 kbar). Figure 1 shows the major element composition of ~10,000 glasses from the global MORB database (blue dots), using the isomolar projections of *Elthon* [1983]. Liquids close to equilibrium with mantle olivine (i.e., molar Mg# (Mg/(Mg + Fe)) > 0.66, shown as red triangles) were last saturated in opx at pressures in excess of 8–10 kbar, in agreement with experimental data [e.g., *Elthon*, 1989; *Elthon and Scarfe*, 1980; *O'Hara*, 1965; *Stolper*, 1980]. The high dissolution rate of opx in undersaturated basalts [*Brearley and Scarfe*, 1986; *Kuo and Kirkpatrick*, 1985a, 1985b] suggests that these melts must be isolated from the surrounding harzburgite during migration to preserve disequilibrium. MORBs also preserve higher light/heavy rare earth element ratios than predicted for equilibrium with residual peridotites dredged from mid-ocean ridges ("abyssal peridotites" [e.g., *Johnson et al.*, 1990]) and sampled in ophiolites [e.g., *Kelemen et al.*, 1995a]. In addition, numerical models of melt migration suggest that the concentrations of trace elements in MORB can also be used to distinguish two-dimensional melt transport from strictly vertical ascent [*Spiegelman*, 1996] when sufficient data become available. Thus major and minor element data indicate that melts migrate through, at a minimum, the shallowest 25–30 km of the mantle with limited chemical interaction.

[5] Some MORBs record melting and rapid extraction from even greater depths. Lu/Hf and Sm/Nd isotopic systematics [*Salters and Hart*, 1989] and $^{230}Th/^{238}U$ excesses [*Beattie*, 1993; *Lundstrom et al.*, 1995; *McKenzie*, 1985] suggest the generation of small melt fractions in the presence of garnet, which is only stable in mantle peridotite at depths greater than ~70 km [*Hirschmann and Stolper*, 1996; *Koga et al.*, 1998]. To preserve the observed excesses of the shortest lived isotopes (i.e., ^{230}Th), melt must be rapidly isolated from the depths where fractionation occurs and delivered to the surface without achieving secular equilibrium or reacting with the majority of the rock through which it passes (see *Kelemen et al.* [1997] for a more complete discussion of melt velocity constraints).

[6] Mantle dunites (>90% olivine) may be the chemically isolated conduits for melt transport. Although residual harzburgites are not in equilibrium with MORB, both the major and trace element concentrations from clinopyroxenes (cpx) in dunites in the mantle section of the Oman ophiolite are in equilibrium with the lavas (very similar to MORB) that formed the overlying crust [*Kelemen et al.*, 1995a]. In addition, spinel compo-

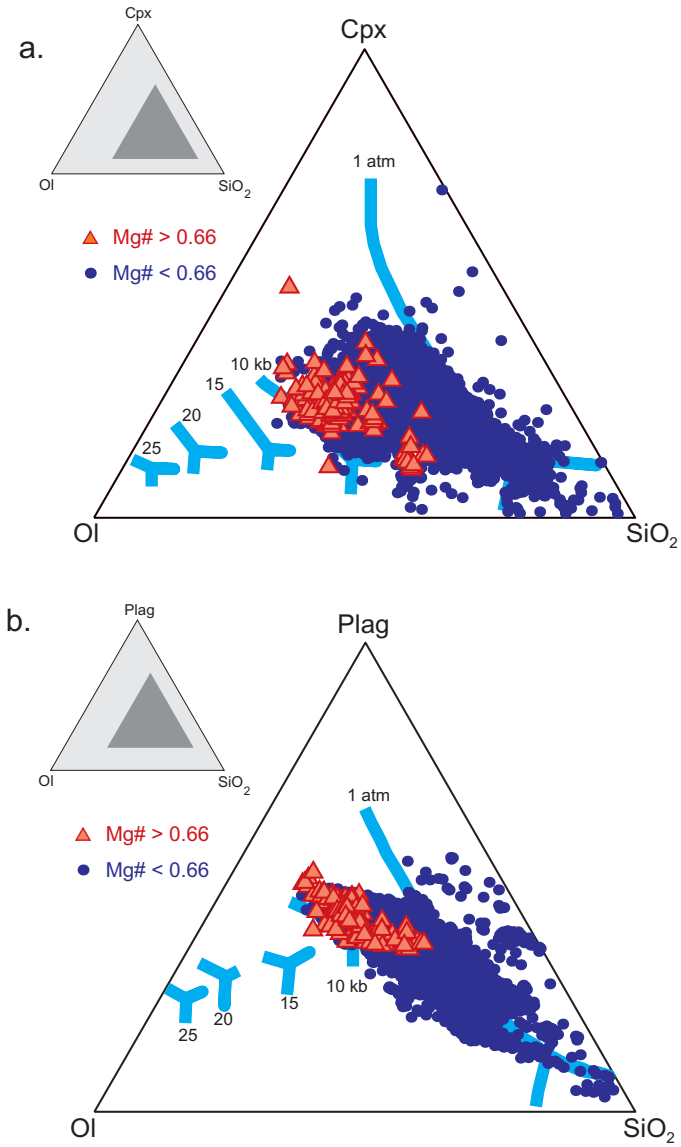

Figure 1. Pressures of equilibration of ~10,000 MORB glasses (circles) as inferred from pseudo-ternary phase diagrams projected from (a) plagioclase and (b) clinopyroxene [after *Elthon*, 1983]. Primitive MORB liquids (triangles), defined by Mg# (Mg/Mg + Fe) in excess of 0.66, were last saturated in orthopyroxene at pressures greater than 10 kb, suggesting these liquids passed through the upper 25–30 km of the mantle without reacting with the surrounding harzburgite. Glass compositions for this global compilation are from the RIDGE PetDB database (http://petdb.ldeo.columbia.edu). The positions of the cotectic lines at all pressures (1 bar - 25kb) are taken from *Elthon* [1983].

sitions from dunites exhibit high Cr/(Cr + Al) and high TiO_2 [*Augé*, 1987; *Kelemen et al.*, 1995a; *Pallister and Knight*, 1981] similar to those found in MORB [*Dick and Bullen*, 1984] and distinct from residual harzburgites [*Allan and Dick*, 1996; *Arai and Matsukage*, 1996; *Dick and Bullen*, 1984; *Dick and Natland*, 1996; *Kelemen et al.*, 1997]. Dunites as observed in the mantle section of the Oman ophiolite, one of the largest, best exposed sections of oceanic crust and mantle, are generally tabular bodies with sharp contacts and orientations subparallel to the foliation in the surrounding harzburgite and the crust-mantle transition zone (paleo-Moho) [e.g., *Boudier and Coleman*, 1981; *Lippard et al.*, 1986]. Contact relationships between dunite and harzburgite (summarized by,

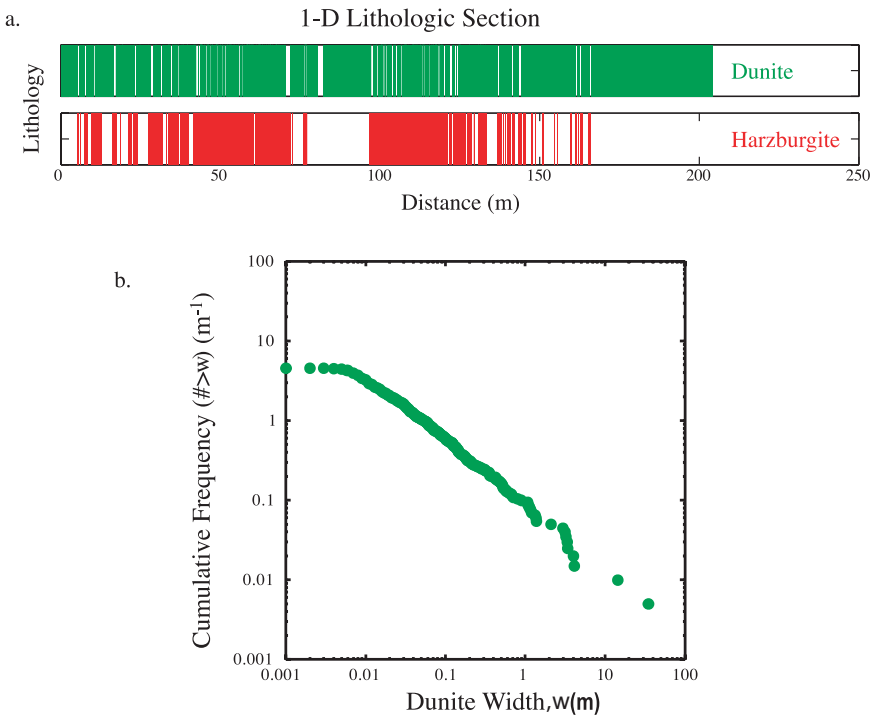

Figure 2. (a) Composite one-dimensional lithologic section of mantle peridotite (containing ~920 individual dunites) from seven outcrops in Wadi Lufti, Oman. Dunite widths range from ~3 mm to 35 m. (b) Dunite size and abundance as measured along the composite section shows a robust power law relationship between dunite width and frequency that extends over more than 4 orders of magnitude. Cumulative frequency is defined here as the number of dunites greater than a given width, *w*.

e.g., *Kelemen et al.* [1995a, Figure 2]) indicate that dunites replaced the surrounding peridotite, via reactions that dissolved pyroxene (and precipitated a similar yet smaller mass of olivine). If the harzburgite foliation developed as the result of deformation associated with "corner-flow" beneath a spreading ridge, then the dunites must have formed in the upwelling mantle beneath the ridge. Thus dunites accommodated chemically isolated transport of melt through the shallow mantle to the base of the crust.

[7] The extent to which dunites are the sole conduits for melt transport is debatable. However, replacive dunites are abundant in the shallow mantle and certainly represent regions of highly concentrated melt flux. As a result, the dunites embody a large part of the time-integrated history of melt migration beneath the spreading center. This study characterizes the abundance and distribution of dunites in the mantle section of the Oman ophiolite to assess (1) viable mechanisms for dunite formation and (2) the ability of a network of dunites to accommodate the observed melt flux to mid-ocean ridges.

2. Observations and Results

2.1. General Field Relations

[8] The Oman ophiolite consists of ~13 large massifs which comprise a nearly continuous band of oceanic lithosphere more than 500 km long and 50–100 km wide. In this study we examine the distribution of replacive dunites exposed in the mantle sections of the Samail and Muscat massifs. Although there are a variety of interpretations of the structural data, detailed mapping efforts in the Samail massif and the adjacent Wadi Tayin massif indicate relatively little internal deformation since the initiation of obduction [e.g., *Jousselin et al.*, 1998; *Nicolas et al.*, 2000], and the peridotites represent residual mantle which passed beneath an oceanic spreading center.

[9] The mantle section of the Wadi Tayin massif preserves a stratigraphic thickness of up to 9–12 km, composed almost entirely of residual harzburgite and dunite [e.g., *Boudier and Coleman*, 1981]. The peridotite is overlain by a 5–7 km thick gabbroic crustal section [e.g., *Pallister and Hopson*, 1981] with a nearly continuous layer of sheeted dikes underlying pillow lavas with compositions very similar to MORB [e.g., *Pallister and Hopson*, 1981; *Pallister and Knight*, 1981]. It is inferred that these observations are applicable to the Samail and Muscat massifs as well, though the crustal section in parts of the Samail massive may have been thinner (~4 km) [*Nicolas et al.*, 1996].

[10] Although the spreading rate during the formation of the Oman crust is unknown, the presence of the continuous igneous crustal layer [e.g., *Nicolas and Boudier*, 1995; *Nicolas et al.*, 2000] suggests a half-spreading rate greater than ~0.05 m/yr. Mid-ocean ridges with spreading rates less than ~0.05 m/yr exhibit extensive exposures of peridotite on the seafloor, especially near fracture zones [e.g., *Cannat*, 1996; *Dick*, 1989]. In addition, there is little evidence for crystal plastic deformation in Oman gabbros [*Nicolas and Ildefonse*, 1996], whereas plastically deformed gabbros are commonly observed along the Mid-Atlantic Ridge [*Cannat et al.*, 1997]. We infer that the Oman ophiolite represents the igneous crust and residual peridotite generated at an intermediate to fast spreading oceanic spreading center.

[11] The majority of dunites in the mantle section of the ophiolite occur as tabular veins, intersecting each other at small angles, with sharp contacts against the surrounding harzburgite. In this study we have chosen exposures that are planar over the length scale of the image and orthogonal to the intersection lineation formed by the planar dunites. Outcrops oriented orthogonal to the ones imaged show no intersections. The widths of dunites range from less than 1 cm to nearly 100 m, and lengths range from less than a meter to several kilometers. To avoid confusion with the large, partially cumulate, dunites formed at the base of the crust, we consider only dunites that are overlain by harzburgite. In some cases, our chosen map areas lie more than 1 km below the crust-mantle transition zone, though this is not possible to verify for outcrops in the Muscat massif.

2.2. Photomosaics and Image Processing

[12] We have measured dunite widths over 4 orders of magnitude (10^{-2} to 10^{2} m). Data were collected using one of several methods depending on scale: one-dimensional (1-D) measured sections, outcrop mosaics for small dunites, hillside/mountainside photomosaics for intermediate scales, and airphoto analysis and chain and compass surveying for the largest dunites.

[13] For the highest resolution, one-dimensional sections were collected in Wadi Lufti (Samail) along a chain line perpendicular to the strike of the predominant dunite orientation/peridotite foliation (335°/65°SW). Seven sample lines ranged in length from 7 to 66 m, for a composite section of 208 m, with every contact along the sample line measured to millimeter precision (Figure 2a).

[14] Dunite distributions over larger length scales are derived from two-dimensional image mosaics. Photomosaics of individual outcrops (Figures 3a and 3b) were constructed from images of 0.5 by 0.5 m areas along a grid superimposed on the outcrop. Lithologic contacts in each image were then retraced and reassembled into the mosaic using Adobe Photoshop. This is an improvement upon the method used by *Kelemen et al.* [2000], exploiting greater overlap, better camera positioning, and less image distortion. The prepared outcrops ranged in size from 3 × 3.5 m to 16 × 5 m, with a final precision of ~3 mm (determined by the width of the marker and the grain size of the rock). Where possible, one-dimensional sections traversed previously analyzed two-dimensional outcrops.

[15] At length scales larger than individual outcrops (Figures 4 and 5), images were gathered and processed in a slightly different manner. For each location, a series of scaled photographs, taken from a fixed point at a known distance from the hillside were digitized and mosaiked, again using

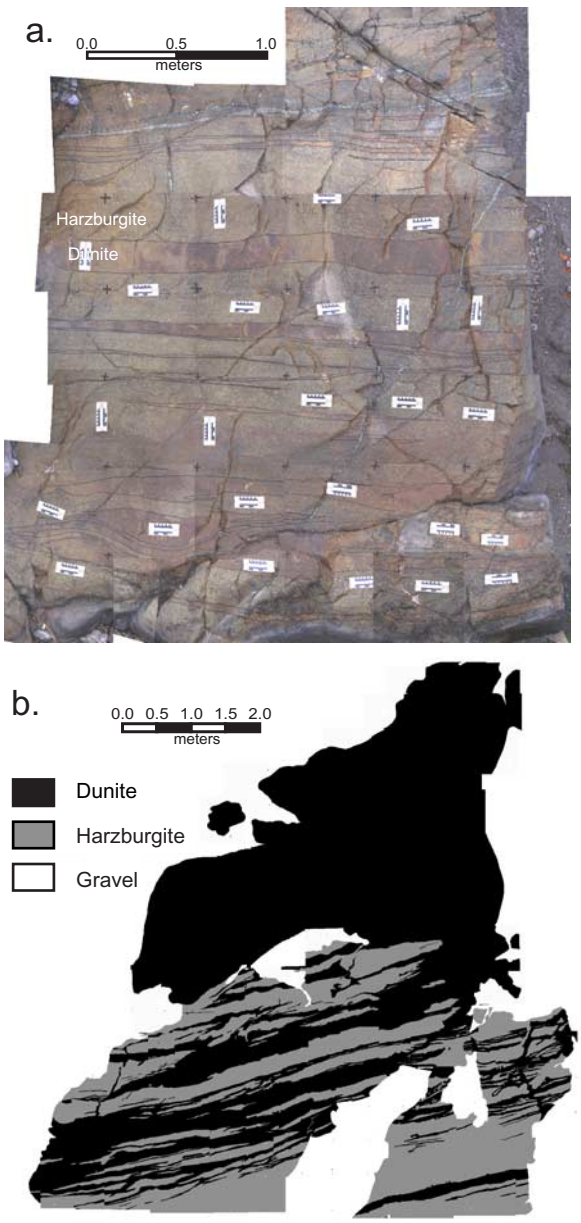

Figure 3. Outcrop mosaics from Wadi Lufti, Oman. The mosaics for (a) Outcrop #10 and (b) Outcrop #18 are composed of ~40 and 170 individual photographs, respectively, taken ~1.5 m above the outcrop surface. Contact information is determined at the outcrop and subsequently digitized from the scaled mosaic.

Adobe Photoshop. The mosaics were printed to large sheets, over which the facies contacts were hand traced, then redigitized. This same process was used for airphoto analysis (Figure 6) to fill in gaps in the ground survey. All mosaics are converted into scaled bitmap (binary) images containing just dunite (or harzburgite) objects for image processing.

2.3. Statistical Analysis

[16] To evaluate the proposed mechanisms of dunite formation and to estimate the total potential flux through dunites, the abundance and distribution of dunites in the melt network must be determined. *Kelemen et al.* [2000] show that the abundance of dunites exhibits a power law dependence on dunite width in the Ingalls ophiolite. In addition, Kelemen et al. extrapolate this dunite size/frequency relationship to predict the abundance of large dunites in the Wadi Tayin massif in Oman.

[17] For the Oman ophiolite, the data from the composite 1-D section in Wadi Lufti show that a robust power law relationship between dunite width and frequency does exist over at least four orders of magnitude in width (Figure 2b). We collected additional dunite width data from images over a wide range of scales using an "intercept width" technique, similar to that used by *Kelemen et al.* [2000]. Dunite widths are measured along parallel lines perpendicular to the dominant dunite strike for each image mosaic. All widths are then corrected for apparent thickness based on field measurements of the true dunite orientation and camera position. In addition, several large dunites were measured using standard chain and compass techniques to further constrain the mosaics. The same width analysis is carried out for the harzburgite images, and therefore the percentage of dunite at each location can be determined by combining the dunite and harzburgite images. To account for the higher number of observations in larger areas, all frequency data are normalized by the total intercept length used in each image. Using cumulative frequency per meter allows for direct comparison of size/frequency data collected at different scales over different size areas. (Using frequency per meter also allows for extrapolation to larger length scales, as will be discussed in section 3.1.)

[18] For each data set, a cumulative distribution function and probability density function can be established from histograms of the width data. The cumulative distribution function (CDF) is defined

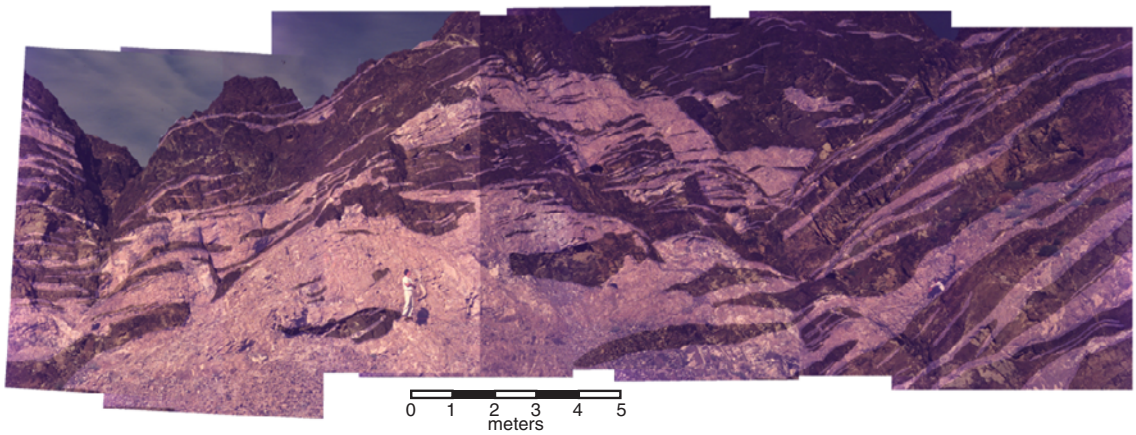

Figure 4. Photomosaic of dunites behind a mosque in Mutrah, part of the Muscat massif. Dunite locations were determined by image analysis and are seen here as the lighter regions in the image. Dunite orientations are measured in the field and used to correct the widths measured from each image.

as the number of objects per meter greater than a given width, w. For a power law, the CDF has the form

$$F_w = \frac{a}{w^D}, \tag{1}$$

where D is the power law exponent and a is related to the proportion of dunite in the image. The probability density function (PDF) is an estimate of the number of dunites of a given width per meter. The PDF is the derivative of the CDF and for the power law above has the form

$$f_w = -\frac{dF}{dw} = \frac{aD}{w^{D+1}}. \tag{2}$$

[19] Ideally, the PDF could be determined directly from the width/frequency histogram. However, the values of both D and a are sensitive to the bin sizes

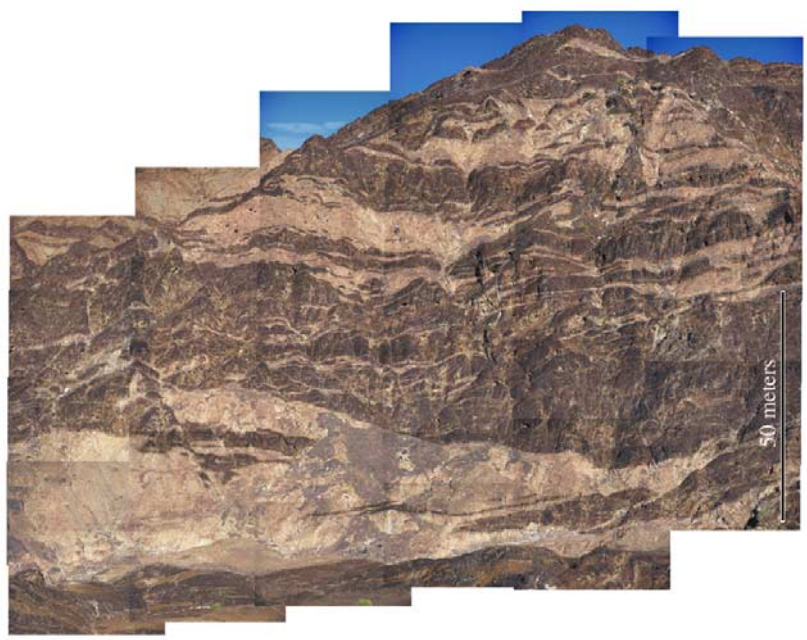

Figure 5. Photomosaic of a mountainside in the Muscat Massif. As at all scales, dunite orientations measured across the image area are used to correct dunite widths as measured from the image mosaic. The lighter rocks are dunite, the darker are harzburgites. The two geologists in the center of the image are standing ~50 m apart.

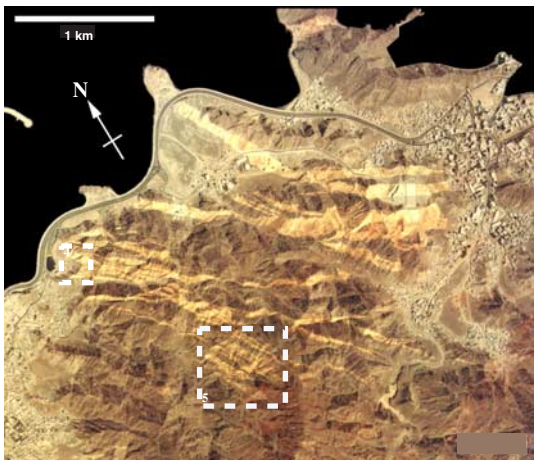

Figure 6. Aerial map of dunites from the Muscat - Mutrah region. Dunites locations were determined by both airphoto analysis and surface observations. Dunites are shown here as highlighted regions superimposed on the airphoto. The locations of Figures 4 and 5 are shown by dashed regions.

used in creating the histogram. Therefore we exploit the mathematical relationship between the distribution functions to calculate the PDF from the more robustly determined CDF.

[20] If the true distribution of dunite widths is indeed scale-invariant over some range of widths, then the abundances of sampled dunites should fall along a common line (Figure 7). However, any sampling of the true population is subject to truncation and censorship errors. Even samples derived from ideal power law distributions will exhibit deviations from perfect power law behavior. Truncation errors occur at the smallest scales since dunite width is limited by the resolution of the image. At the larger scales, object width is limited by the size of the area of interest. In addition, censorship can systematically diminish the sampling frequency. At the grain scale (0.5–3 cm) it is very difficult to distinguish the matrix of olivine around pyroxenes in the harzburgite from a discrete dunite vein. Even though all widths are subject to this precision limit, small-scale features are most affected, since the error is a larger fraction of the true width. At the largest scale, the widths of dunites with one boundary outside the field of view are also underestimated. This type of censoring can occur for any object but is more likely for larger objects and more important for rare observations. For a combination of these reasons, the number of the largest and smallest dunites are underestimated. Several corrections have been developed to account for these errors in cumulative frequency plots [e.g., *Barton and Zoback*, 1992; *Laslett*, 1982]. However, the effects of the corrections are minimal if the relationship is measured from the central linear portion of the distribution [*Pickering et al.*, 1995], which comprises the majority of the data. We define the central portion of the distribution as data that lie within the 80th percentile of absolute range from the median.

[21] Values of D and a are obtained from the culled CDF data using a linear regression with data weighted by the studentized residuals to eliminate outliers with high leverage. We initially fit the linearized system, $\log F = \log a - D \log w$, using a least squares method. Outliers are culled based on the value of their studentized residuals, and the retained data are refit. In all cases, the retained data (Figure 8, open circles) represent ~80% of the total data set. For a more complete description, see *Weisburg* [1985, p. 109–117]. Values of the fitted

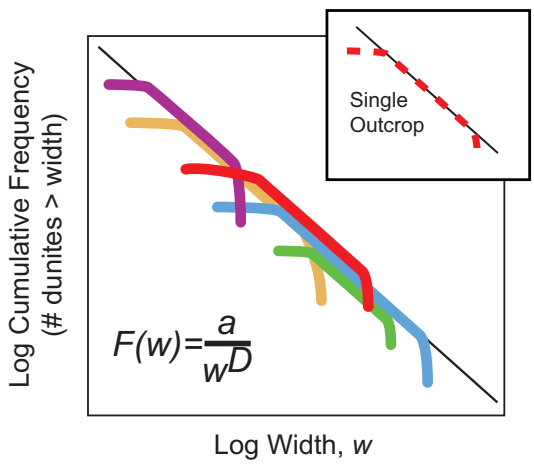

Figure 7. Idealized scale-invariant power law distribution. This illustration demonstrates the how several data sets over a range of overlapping length scales can be used to determine the true power law distribution of the dunite population. Individual outcrops exhibit a characteristic relationship between log width and log frequency (inset). If the distribution of dunite widths is scale-invariant, then every outcrop will lie along a common line.

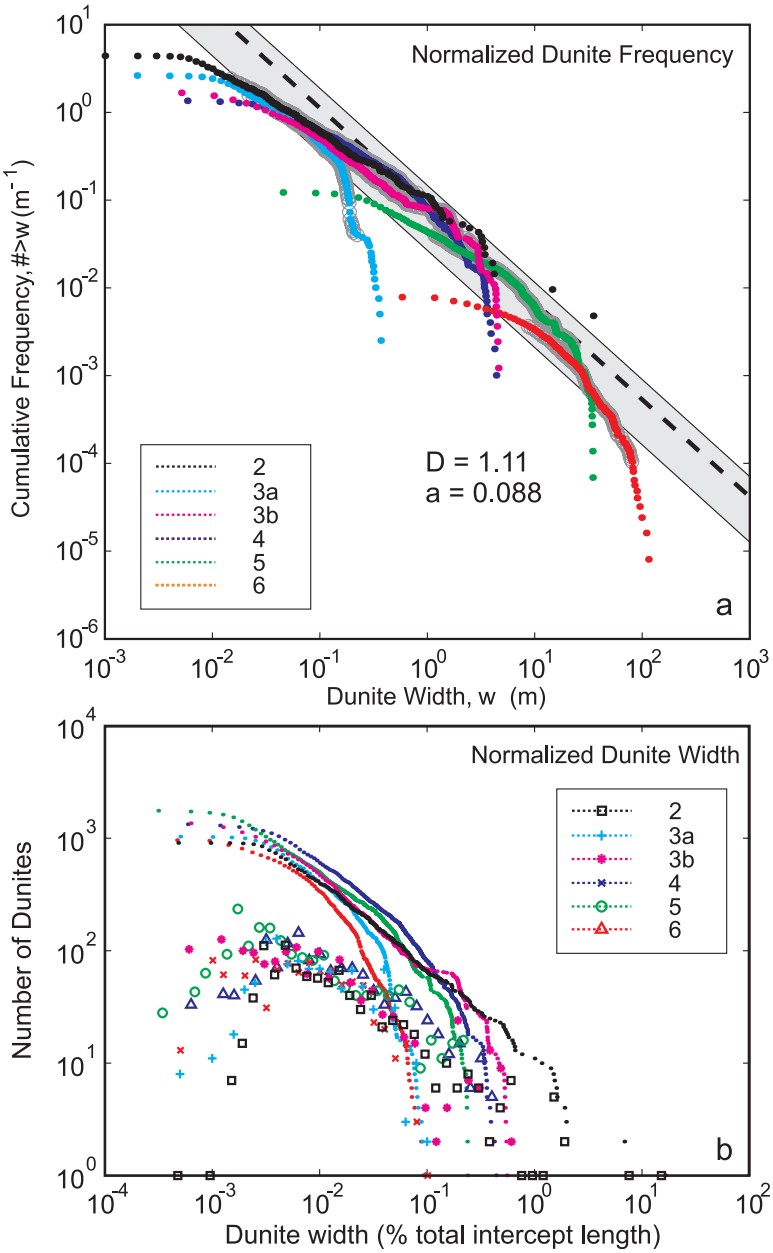

Figure 8. Width distribution data from dunites in the mantle section of the Oman ophiolite. These data (dots) are collected from lithologic sections and photomosaics with length scales spanning more than 4 orders of magnitude. (a) To reduce the effects of truncation and censorship errors, only data within 80% of the range from the median value (circled) are used in the fits. The mean of the fits to the individual data sets is shown by the gray band (dashed line ±1 σ in a to account for differences in dunite density between images). (b) Width-normalized dunite size/frequency statistics. Although difficult for extrapolation to larger length scales, normalization of dunite width the total intercept length collapses the data sets onto each other. In addition to the CDF data, the binned PDF data are shown with discrete symbols corresponding to each image.

parameters for individual locations, as well as their average ($D = 1.11$, $a = 0.088$), are shown in Table 1. For a given dunite size, there exists 10^D, or ~13 times as many dunites of that size compared to the number of dunites that are an order of magnitude wider. The CDFs for the data collected in Oman fall on a common distribution line spanning ~4 orders of magnitude. (Figure 8, gray band) Because the areas mapped in detail have variable percentages of dunite (18–68%), individual data sets may

Table 1. Fit Parameters Derived From Each Dunite Image Presented in This Study, Including the Least Squares Correlation Coefficient, R^2[a]

	Figure	D	a	R^2	% dunite
Lufti 1-D composite	2	0.78	0.098	0.99	65.7
Lufti o/c #10	3a	1.38	0.014	0.83	68.2
Lufti o/c #18	3b	0.78	0.075	0.98	49.9
Mosque	4	1.07	0.079	0.98	45.5
Mountainside	5	1.00	0.061	0.96	44.3
Muscat Airphoto	6	1.64	0.198	0.98	17.7
Parameter Mean		1.11	0.088		

[a] For each image, the corresponding figure number and percentage of dunite in the image are also listed. The details of the parameter fitting are described in the text.

fall above or below the average line, reflected in the value for a. For this reason we use the mean values of D and a for extrapolation to larger length scales.

3. Discussion

[22] Dunite melt conduits as observed in the shallow mantle section of the Oman ophiolite range in size from less than 1 cm to nearly 100 meters. In addition, the abundance of these dunites exhibits a power law dependence on width as measured over 4 orders of magnitude. In the section 3.1, we use size/frequency distribution of dunites as measured in Oman to assess the proposed mechanisms for the formation of replacive dunites and subsequently estimate the total unequilibrated melt flux a dunite network can accommodate beneath an oceanic spreading center.

3.1. Extrapolation to the Melting Region

[23] By extrapolating the power law size frequency distribution measured in this study, we can estimate the size and abundance of dunite melt conduits over larger length scales (i.e., the melting region beneath mid-ocean ridges). The CDF data are normalized per unit of observation length to enable comparison of data from regions of different size. This normalization also allows for easy extrapolation, simply by multiplying the distribution function by the desired length scale, L. Therefore the number of dunites wider than w predicted in L meters of observation perpendicular to the general strike of the tabular dunites is defined as

$$F_w = \frac{a}{w^D} L. \tag{3}$$

[24] Extrapolation in this manner adequately predicts the abundance of the largest dunites observed in individual massifs in Oman (L = 10 km) as reported by *Kelemen et al.* [2000] (Figure 9). Estimating dunite abundance over length scales commensurate with the melting region beneath mid-ocean ridges requires 1 order of magnitude of additional extrapolation (L = 100 km). This approach suggests that there may be at least one dunite as wide as ~3.5 km in the melting region beneath an oceanic spreading center (Figure 9). A dunite of this width, even with a 3–5% steady state melt fraction, is as yet undetectable by seafloor broadband seismic networks [*Hung et al.*, 2000]; so unfortunately, this hypothesis cannot be tested. Alternatively, there could be

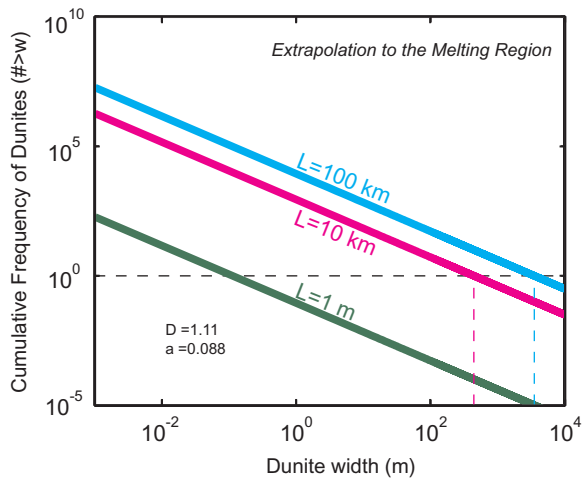

Figure 9. Extrapolation for dunite abundance to larger length scales using the power law size/frequency distribution determined from the dunite width data from Oman. For length scales on order of individual massifs in Oman, (10 km) the extrapolation predicts dunite abundances consistent with field observations (red dashed line) [*Kelemen et al.*, 2000]. Extrapolation to length scales commensurate with the melting region beneath mid-ocean ridges (100 km) predicts the existence of dunites as wide as several kilometers (blue dashed line). Alternatively, perhaps the larges dunites are no larger than the widest dunites we observe in Oman (~100 m).

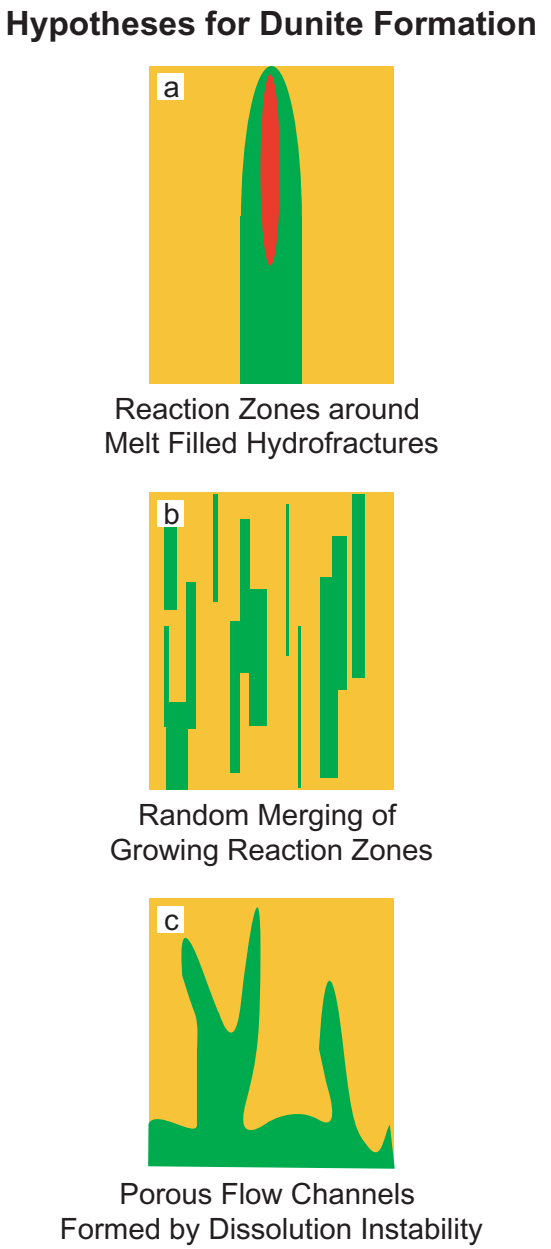

Figure 10. Three hypotheses for replacive dunite formation in the shallow mantle based on reaction of silica-undersaturated basalts with shallow mantle harzburgites. (a) Dunites may form as diffusive reaction zones around melt filled hydrofractures. (b) Random merging of growing reaction zones may give the appearance of large dunites. (c) Dunites may form by a reactive infiltration instability creating high porosity dunite melt conduits.

a smaller maximum size limit. The widest dunites observed in the Oman mantle section (~100 m) could be the largest present beneath mid-ocean ridges.

3.2. Mechanisms of Dunite Formation

[25] Dunites have been hypothesized to form by (1) diffusive reaction around melt-filled hydrofractures [*Nicolas*, 1986, 1990; *Suhr*, 1999], (2) random merging of growing reaction zones around several hydrofractures [*Kelemen et al.*, 2000], and (3) a reactive infiltration instability resulting in high porosity conduits. [*Aharonov et al.*, 1995; *Kelemen and Dick*, 1995; *Kelemen et al.*, 1995b; *Spiegelman et al.*, 2001] (Figure 10a–10c). For all three hypotheses, replacive dunites are formed by reaction between ascending MORB melts and the surrounding peridotite. As pressure decreases, the solubility of silica-rich phases (opx and cpx) in basalt increases [*Dick*, 1977; *Quick*, 1981; *Kelemen*, 1990]. Therefore ascending melts dissolve pyroxene and precipitate olivine, increasing the liquid mass and, where the time integrated melt flux is large enough, creating dunite in their wake [*Daines and Kohlstedt*, 1994; *Kelemen*, 1990; *Kelemen et al.*, 1995b]. Kinetic studies show that these reactions can occur rapidly [*Brearley and Scarfe*, 1986; *Kuo and Kirkpatrick*, 1985a, 1985b; *Zhang et al.*, 1989]. The discriminating difference between hypotheses is the melt transport mechanism. In hypotheses 1 and 2, pyroxene-undersaturated melt within hydrofractures forms dunite along the margins as the melt reacts with the wall rock. In hypothesis 3, there is no crack, and high porosity dunite channels form as a result of a dissolution instability. The increased porosity resulting from the dissolution reaction increases the local permeability, which in turn increases the melt flux to the area. The increased flux draws in more undersaturated melt, resulting in further dissolution.

3.3. Dunites as Diffusive Reaction Zones

[26] Dunite growth as reaction zones around melt filled hydrofractures is limited by silica diffusion in the melt. Whether in hydrofractures or in the surrounding porous rock, buoyancy-driven melt transport is predominantly vertical, whereas, dunite margins grow in the direction orthogonal to melt transport. Since the kinetics of pyroxene dissolution are fast, silica must be continually moved from the reaction front back to the hydrofracture in order to drive continued dissolution. Because the melt

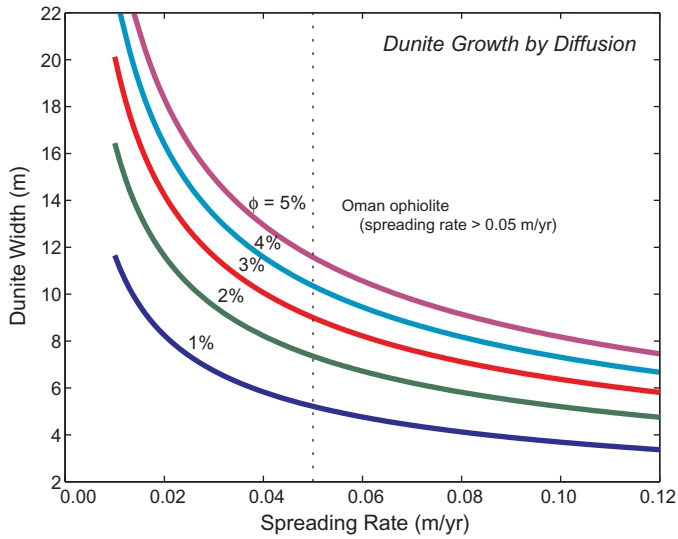

Figure 11. Width of dunite reaction zones around melt filled hydrofractures as a function of spreading rate. As spreading rate increases, the time available for diffusive transport of material in the melting region decreases. For moderate porosities and spreading rates greater than 5 cm/yr, dunites wider than ~12 m cannot form by diffusion around a melt filled hydrofracture within the residence time of solid material in the melting region. To maximize the time for diffusion, these calculations assume dunites begin forming at the base of the melting region and remain active until reaching the surface.

transport velocity in the host peridotite is small (~1 m/yr [e.g., *Kelemen et al.*, 1997]), hydrodynamic dispersion will also be very small [*Freeze and Cherry*, 1979]. Therefore dunite growth is limited by the lateral transport of silica by diffusion.

[27] This is a limiting case with no horizontal advection of melt. Focused flow networks require that melt, initially formed along grain boundaries uniformly distributed in a porous source rock, flows laterally into channels of focused transport. This lateral advection into the channels (10^{-1}–10^{-4} times the vertical velocity of ~1 m/yr in porous models [*Spiegelman et al.*, 2001]) may be generally faster than the diffusive transport velocity of SiO_2.

[28] If dunites are diffusive reaction zones, then the time required for formation via Fickian diffusion can be estimated by

$$\frac{dC}{dt} = -D_{\text{eff}} \frac{d^2C}{dw^2}. \tag{4}$$

Assuming the melt composition in the hydrofracture (i.e., degree of undersaturation) remains constant, the dunite width, w, is proportional to the square root of the formation time, t. The effective diffusivity, D_{eff}, of a particular species in the two phase system is defined as [*Crank*, 1975]

$$D_{\text{eff}} = \phi D_{\text{melt}} + (1 - \phi) D_{\text{rock}}, \tag{5}$$

where ϕ is the interconnected porosity and D_{melt} and D_{rock} are the diffusivities of silicon in the melt and solid phases, respectively. Given a moderate porosity of 1–3%, $D_{\text{melt}} \approx 10^{-11}$ m^2/s, and $D_{\text{rock}} \approx 10^{-15}$ m^2/s [*Lesher et al.*, 1996], the time required to form the largest observed dunites in Oman (~100 m) is 250–750 Ma. However, the lifetime of solid material rising through the melting region beneath a spreading center is only ~1–10 Ma for spreading rates of 0.12–0.01 m/yr, respectively. Therefore the widest dunites that could be formed by diffusion around melt-filled hydrofractures are ~3–20 m (depending on porosity and spreading rate) (Figure 11). If the spreading rate during the formation of the igneous crust in Oman was at least 0.05 m/yr, then dunites wider than ~3–10 m could not be formed as the result of diffusion alone.

3.4. Dunites as Merging Reaction Zones

[29] Large dunites (>10 m wide) are present in the Oman ophiolite in the abundances predicted by the

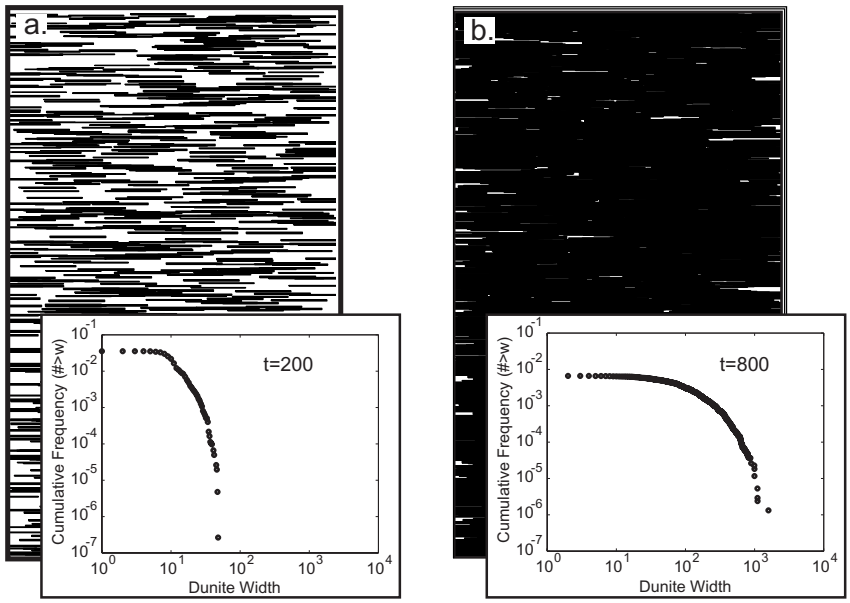

Figure 12. Forward model of merging reaction zones around melt filled hydrofractures. An initially spatially random set of five cracks of width 1 are allowed to grow diffusively with the square root of time. At each timestep, five new cracks randomly nucleate and begin to grow. (a) At time t = 200, a weak power law begins to form, but dunite widths span less than 2 orders of magnitude. At this point, dunites occupy ~42% of the total area. (b) By t = 800, dunite widths range ~3 orders of magnitude, but now 94% of the total area is occupied by dunites. Although merging of growing reaction zones as shown here can produce very wide dunites, the abundance statistics are not consistent with the field observations.

observed power law (~10/km). However, diffusion around individual melt-filled hydrofractures cannot explain their formation. In modeling dunite formation as reaction zones around a static distribution of cracks, *Kelemen et al.* [2000] suggested that wide dunites may be the result of random merging of reaction zones around individual hydrofractures.

[30] To test this hypothesis, we examined a series of forward models in which reaction zones around dunites are allowed to grow and merge and compared the results to the distribution of observed dunite widths in Oman. These models start with an initial, spatially random distribution of five parallel cracks. Reaction zones around each crack grow with the square root of time. In addition, five new dunites nucleate at each time step (unlike *Kelemen et al.* [2000]). With time, the merging of reaction zones creates increasingly wider dunites, and a weak power law size/frequency distribution begins to emerge. However, the merging process fills space rapidly. After 200 time steps, the largest dunites are only ~20 times wider than the initial width, but the dunites occupy ~ 42% of the total area (Figure 12a). By the time very wide dunites (>10^3 times the initial width) form, more than 94% of the model space is filled with dunite and the power law has degraded (Figure 12b).

[31] We examined a range of growth and nucleation rates, which affect the time required to fill space with dunites, but in all cases, the range in dunite size never spanned more than 1.5 orders of magnitude before dunites filled more than 50% of the available space. Additional model parameters could be added to modify the fracture mechanics or diffusive growth as a function of dunite width (i.e., new dunites may preferentially nucleate near larger dunites, or larger dunites may grow faster). Such feedback effects may produce a power law size/frequency distribution over several orders of magnitude in width, by analogy with the feedback mechanisms examined for purely porous conduits in the next section of this paper. However, there is as yet no evidence to suggest either of these is necessary. Preliminary size/frequency data for harzburgites (the space between dunites) in the images presented here exhibit exponential distributions,

suggesting the random spatial distribution of dunites within the areas we mapped in detail. (We have concentrated on areas with high dunite density and suspect that on the massif and ophiolite scale, dunites may be clustered in a nonrandom fashion.) Regardless of the nature of the spatial distribution, the diffusion equation (4) specifies that the growth rate for any given dunite should decrease with time, preventing larger dunites from growing faster.

3.5. Dunites as Porous Conduits

[32] Dunites may represent high porosity melt channels formed as a result of the reactive migration of melt in a solubility gradient [*Aharonov et al.*, 1995; *Kelemen and Dick*, 1995; *Kelemen et al.*, 1995b; *Spiegelman et al.*, 2001]. As melt migrates upward, it becomes progressively undersaturated in pyroxene. The resulting reaction between the melt and harzburgite dissolves pyroxene and precipitates olivine while increasing the liquid mass [*Daines and Kohlstedt*, 1994; *Kelemen*, 1990; *Kelemen et al.*, 1995b]. The increased porosity increases the local permeability, which in turn increases the melt flux to the area. The increased flux draws in more undersaturated melt, resulting in further dissolution. Numerical models of this positive feedback, or reactive infiltration instability, indicate that a self-organized network of high porosity dunite conduits, coalescing downstream, can rapidly form within the melting region [*Aharonov et al.*, 1995; *Spiegelman et al.*, 2001]. Modeled widths of these porous conduits, measured in terms of the width over which the soluble solid phase has been completely removed by dissolution, are ~1 km wide when scaled to the size of the melting region beneath mid-ocean ridges.

[33] The primary requirement of the melt transport process is that it provides a sufficient flux of unequilibrated melt to the ridge axis to form the oceanic crust. We can assess the ability of a high-porosity dunite network to accommodate this flux using the dunite size/frequency relationship established from our field observations. The total melt flux to the ridge can be estimated as the product of the crustal thickness, half-spreading rate, and ridge length. Assuming a constant global crustal thickness of 6 km, the estimated melt flux to the ridge is 60–900 m^3/yr per meter of ridge segment along axis for slow and fast spreading ridges (0.01–0.15 m/yr), respectively.

[34] The total flux through the dunite network can be estimated by integrating the predicted flux in a dunite of a given size with the observed size/frequency data. The 2-D flux (volume per unit time per unit length) in an individual dunite, J_w, can be defined as

$$J_w = \phi v w, \tag{6}$$

which is the product of the dunite width, w, and the Darcy flux

$$\phi v = \frac{k \Delta \rho g}{\eta}, \tag{7}$$

where $\Delta\rho g$ is the driving pressure gradient due to melt buoyancy, η is the melt viscosity, and the permeability, k, is a function of porosity, ϕ, grain size, d, and geometry, C:

$$k = \frac{\phi^n d^2}{C}. \tag{8}$$

For an interconnected porous network around tetrakaidecahedral grain edges, $n = 2$ and $C = 1600$ [*von Bargen and Waff*, 1986]. The grain size, d, is assumed to be ~4 mm, consistent with the observations from dunites in Oman [*Boudier and Coleman*, 1981]. The driving pressure gradient is derived from the density difference, ~500 kg/m^3, between basaltic melt and olivine. The total flux of the system, J_{tot}, is the integral of the product of the flux function, J_w, and the dunite PDF, f_w, over the range of dunite sizes predicted for the given length scale, L, where

$$J_{tot} = \int_{w_{min}}^{w_{max}} J_w f_w dw \tag{9a}$$

$$J_{tot} = \int_{w_{min}}^{W_{max}} \phi v w \frac{aD}{w^{D+1}} L dw. \tag{9b}$$

[35] To estimate the total flux through all dunites, the minimum bound for the integral, w_{min}, is

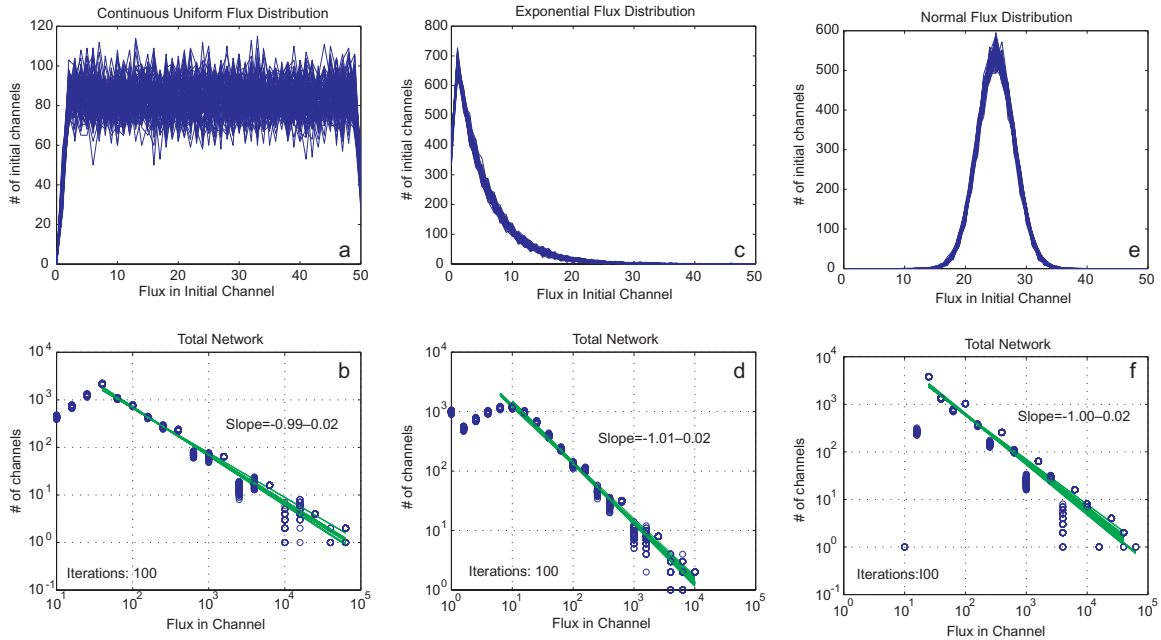

Figure 13. Relationship between flux and number of channels for a system of binary merging conduits for different initial flux distributions: continuous uniform, exponential, Gaussian. In each case a starting population of ~4000 channels, with flux distributions shown in the upper panels (Figures 13a, 13c, and 13e), is allowed to randomly merge in pairs. Merging continues until all the flux is carried in one channel. The probability density function (PDF) of the resultant network in each run (Figures 13b, 13d, and 13f) is below each initial distribution. This process was repeated 100 times for each of the different initial distributions. In all cases, the maximum flux in any initial channel is constant (50 times the minimum flux in runs shown here), and the total flux through the system is constant. In all cases, there exists a robust power law relationship, with a slope of −1, between flux and number of channels. This relationship holds over nearly 4 orders of magnitude, regardless of the initial distribution of flux or order in which channels merge.

equivalent to the width of the smallest observed dunite (~1 cm). The upper integration bound, w_{max}, is determined from the extrapolation of the power law at the length scale of the melting region. However, as discussed above, only dunites greater than the length scale of diffusive equilibration can preserve chemical disequilibrium. Therefore the total flux of unequilibrated melt, J_{uneq}, occurs only through dunites wider than 3–10 m.

[36] In addition, we assume that the dunites form a network of channels that coalesce downstream. As discussed by *Kelemen et al.* [2000], this is consistent with, though not required by, the observed power law relationship between dunite width and frequency. In such a network, flux must be conserved where porous conduits merge. In systems where flux is conserved at binary intersections the number of channels is inversely proportional to the flux they carry, or $f_w \propto J_w^{-1}$ [e.g., *Hart*, 1993]. In its simplest form, at each intersection, two channels each carrying one unit of flux join to form one channel carrying twice the flux.

[37] Using a series of stochastic models, we show that this relationship between the number of channels and the flux they carry holds regardless of the initial distribution of flux or the order in which channels merge. In each case, ~4100 channels are initially assigned a flux according to a particular probability density function, continuous uniform, exponential, or gaussian, with a fixed maximum allowable flux ranging from 1–100 times the smallest initial flux (Figures 13a, 13c, and 13e, respectively). The channels randomly merge in pairs until all the flux is in one

channel. This process is repeated 100 times for each class of initial flux distribution. For any given maximum initial flux, the total flux through the system is constant, regardless of the shape of the initial distribution. In all cases, the number of channels is inversely proportional to the flux they carry as measured over ~4 orders of magnitude (Figures 13b, 13d, and 13f). This consequence of flux conservation is also observed in theoretical [*Aharonov et al.*, 1995] and numerical [*Spiegelman et al.*, 2001] models of reactive porous flow, where $f_w \propto J_w^{-1}$.

[38] Our dunite size/frequency observations from Oman indicate that $f_w \propto w^{-(D+1)}$. Equating these relationships for f_w suggests that flux is nonlinearly proportional to dunite width, or

$$J_w \propto w^{D+1}.$$

Using this width-flux relation, we can define a porosity scaling as a function of dunite width. After substitution of equation (6) into the above relation, it follows that

$$\phi v w \propto w^{D+1}$$

Canceling w from both sides and substituting equation (8) into equation (7) yields the following relationship between porosity, ϕ, and channel width, w:

$$\frac{\phi^n d^2}{C\eta}\Delta\rho g \propto w^D.$$

Assuming grain size, d, melt viscosity, η, grain boundary geometry, C, or the driving pressure gradient, $\Delta\rho g$, do not vary significantly between dunites of different sizes, the only free parameter is the interconnected porosity. Therefore, by specifying the maximum porosity, ϕ_{max}, in the largest dunite, w_{max}, the porosity in any given dunite can be written as

$$\phi = \phi_{max}\left(\frac{w}{w_{max}}\right)^{D/n}. \quad (10)$$

The Darcy flux equation (7) can then be expressed as

$$\phi v = \frac{\phi_{max}^n d^2 \Delta\rho g}{C\eta}\left(\frac{w}{w_{max}}\right)^D. \quad (11)$$

After substitution of equation (11) into equation (9b), if flux is nonlinearly proportional to dunite width, the total flux can be expressed as

$$J_{tot} = \frac{\phi_{max}^n d^2 \Delta\rho g a D L}{C\eta w_{max}^D}(w_{max} - w_{min}). \quad (12)$$

[39] Adopting the spreading rate constraint for Oman, we assume that all flux through dunites wider than 5 m will preserve disequilibrium between migrating melt and the surrounding harzburgite. For length scales commensurate with mid-ocean ridge spreading centers (L = 100 km), the largest dunites in the network may be as wide as ~3500 m. Given a maximum porosity in the widest dunites of 1–3%, the total flux through the dunite network is comparable to the observed ridge flux (Figure 14a). More importantly, the flux of unequilibrated melt accounts for greater than 99% of the total melt flux. Alternatively, if the largest dunite widths in the melting region are limited to the widest dunites observed in Oman (w_{max} = 100 m), this "nonlinear flux model" (Figure 14b) still supplies a sufficient unequilibrated melt flux (~95% of the total flux) to satisfy the mid-ocean ridge constraints at reasonable porosities (ϕ_{max} < 4%). These results indicate that melt transport through dunites wide enough to preserve disequilibrium with the shallow mantle can be accommodated entirely by porous flow, and thus there is no requirement for transport through melt-filled cracks.

[40] Flux conservation is a necessary constraint on the melt flux model. A "linear melt flux" model that assumes a constant Darcy flux (e.g., integration of equation (9b) assuming the porosity in channels is constant and therefore independent of dunite width), does not reproduce the observed fluxes of unequilibrated melt at mid-ocean ridges. The total ridge flux in the "linear melt flux" model can be accommodated if all dunites have porosities of 1–2%. However, the unequilibrated melt flux accounts for only ~34% of the total flux, if the maximum dunite width is 3578 m (Figure 15a), and only 22% of the total flux if the maximum dunite width is 100 m (Figure 15b). Such volumes of equilibrated melt would result in an andesitic composition for the

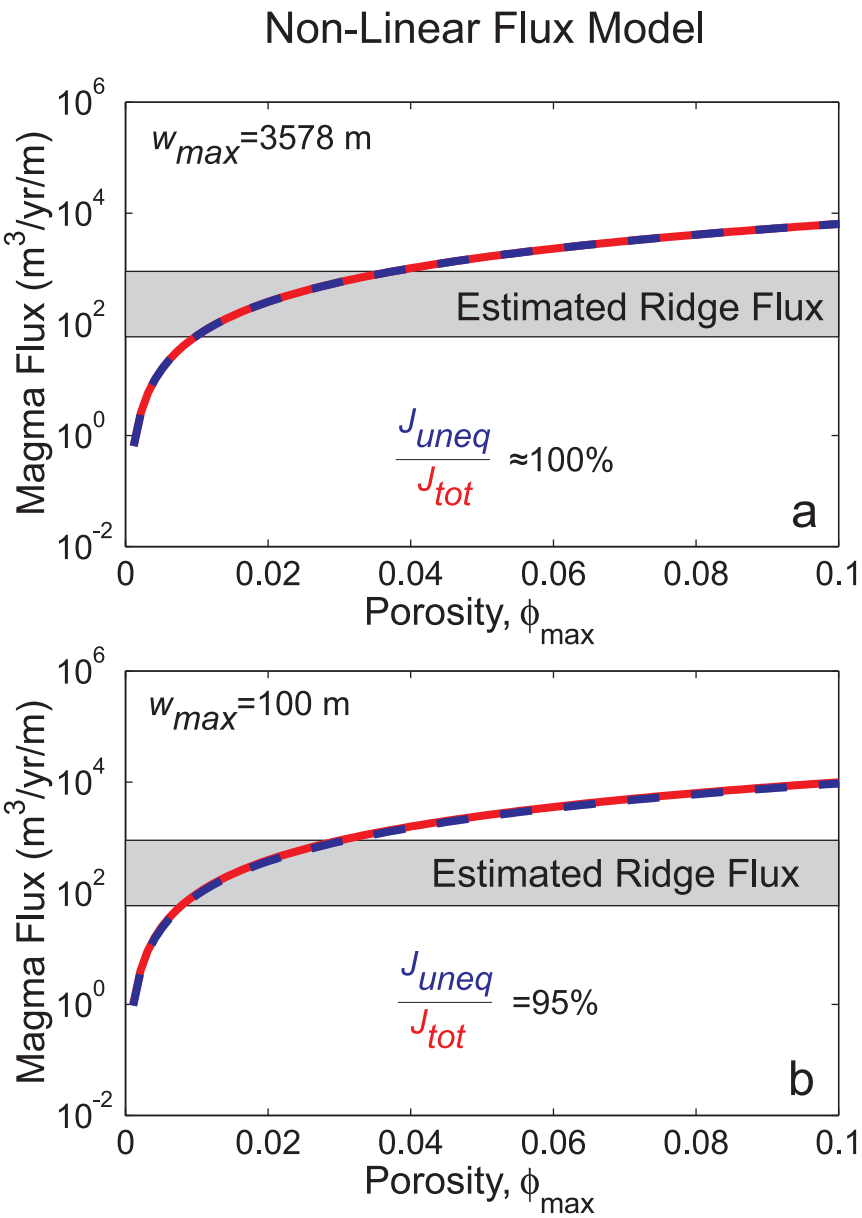

Figure 14. Calculated melt flux through a porous dunite network as a function of porosity, given the power law abundance relationship derived from field observations. These calculations assume that only dunites wider than 10 m can accommodate chemically unequilibrated melt flux. These "non-linear flux model" calculations incorporate the flux conservation constraint. (a) If the largest dunites have widths predicted by the power law for a length scale of 100 km, the unequilibrated flux (J_{uneq} - dashed line) is nearly 100% of the total flux (J_{tot} - solid line) through the system and satisfies the observed ridge flux constraint (gray field) over a range of moderate porosities. (b) If the largest dunites are limited to the widest dunites observed in the mantle section of the Oman ophiolite (100 m), the observed ridge flux constraint is still satisfied.

igneous oceanic crust, corresponding to a liquid composition in equilibrium with olivine, pyroxene, and spinel in the shallow mantle immediately below the base of the crust (~2 kb), very different from the observed basaltic bulk composition of oceanic crust and primitive MORB (Figure 1). Thus dunite channels can only accommodate the flux of unequilibrated melt through the shallow mantle if the

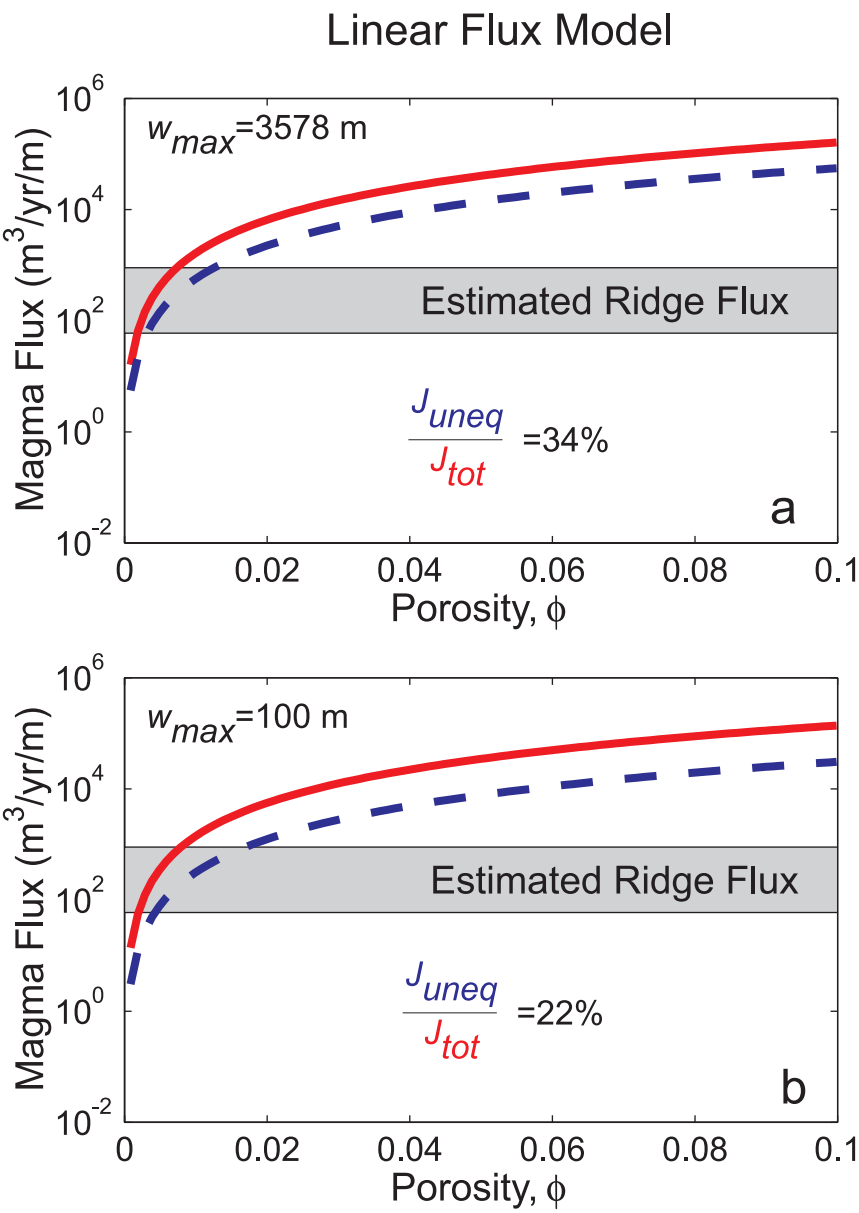

Figure 15. Calculated melt flux through a porous dunite network in which all dunites have a single porosity. (a) The "linear flux model" with the maximum width suggested by extrapolation of the power law predicts the unequilibrated flux (dashed line) accounts for only 34% of the total flux (solid line). (b) The unequilibrated flux accounts for only 22% of the total flux if the maximum dunite width is limited to the widest observed dunites in Oman, ~100 m. In either case, the predicted fluxes satisfy the observed ridge flux constraint (gray field) over a narrow range in porosities less than ~1–2%.

porosity within the dunites is proportional to their width.

4. Conclusions

[41] Dunite widths as measured in the mantle section of the Oman ophiolite exhibit a scale-invariant power law size/frequency distribution over 4 orders of magnitude. The power law slope ($D \approx 1.1$) predicts that there exist ~13 times more dunites for every order of magnitude decrease in dunite width. Extrapolation to larger length scales is consistent with field observations at the massif scale and suggests that dunites as wide as 3.5 km

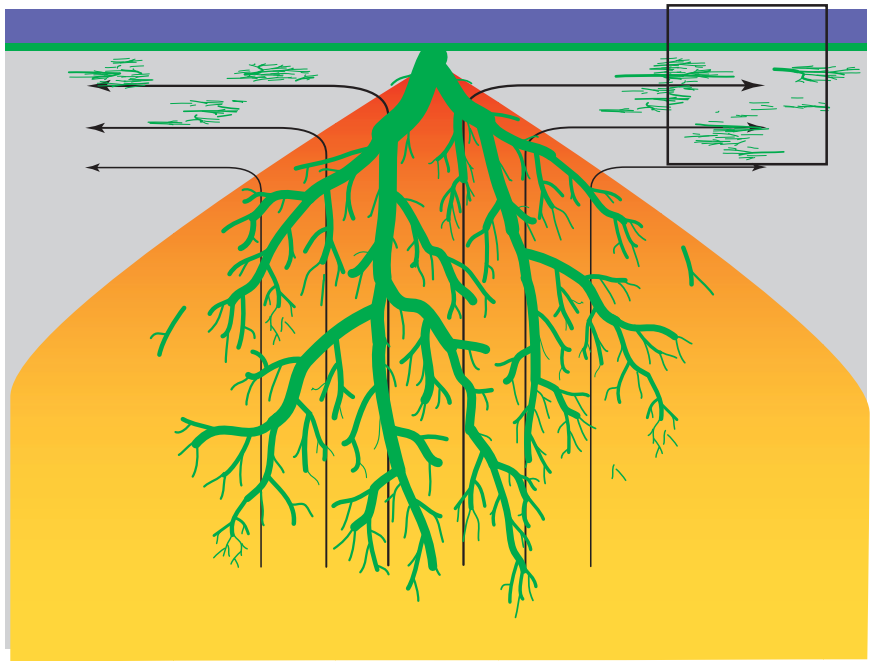

Figure 16. Schematic illustration of a coalescing dunite network beneath an oceanic spreading center based on observations in the Oman Ophiolite. Dunites are shown in green, the crust in blue, and melt is presumed to be present throughout the red and yellow region. The box in the upper right corner indicates the scale of the lithologic section preserved in Oman. The preserved dunites may have been thinned, for example, via simple shear, during transposition resulting from corner flow. We have implicitly assumed that this thinning affected all dunite widths by the same percentage. Thinning in this manner would affect the magnitudes of the dunite widths but not change the ratio of smaller dunites to larger ones. Therefore the power law slope would remain unaffected.

may exist in the melting region beneath oceanic spreading centers. Alternatively, dunites may never exceed 100 m, equivalent to the width of the largest dunites we observe in the Oman mantle section.

[42] Diffusive reaction zones around individual melt-filled hydrofractures cannot explain the formation of wide dunites, as the time required to form the largest observed dunites is greater than the transport time of solid material through the melting region. For the inferred minimum spreading rate of the spreading center that formed the Oman ophiolite, dunites more than $\sim$3–10 m wide could not have been formed by this process. Forward models for the formation of wide dunites by the random merging of reaction zones rapidly fill space and do not generate the power law relationship observed in the field. Instead, our data are most consistent with the formation of dunites as a network of high porosity dissolution channels.

[43] We use the dunite width/frequency statistics and diffusive equilibration length constraints to estimate the total flux of melt through porous dunite channels to the ridge axis. In a system of coalescing channels that conserves flux, porous flow in dunite dissolution channels can accommodate the observed melt flux to the ridge over a wide range of spreading rates and moderate porosities and can preserve the observed disequilibrium between ridge basalts and the shallow, residual mantle.

[44] On the basis of our observations of dunite shape, size, abundance, and distribution, we offer the following schematic illustration of the melt migration network beneath a spreading center (Figure 16). In the melting region beneath a spreading center, ascending melts have the potential to dissolve pyroxene and precipitate olivine, leaving dunite in its wake. These high porosity dunite channels coalesce upward and toward the ridge axis. Merging increases dunite width and porosity while decreasing the number of conduits, thus focusing melt transport toward the ridge axis.

Acknowledgments

[45] We would like to thank Greg Hirth, Marc Parmentier, Jack Whitehead, and Maria Zuber for a thorough examination and insightful comments regarding this work, as well as Günter Suhr, Kazuhito Ozawa, and Susumu Umino for their thoughtful reviews. This work was funded by a NSF Graduate Research Fellowship and NSF grants OCE-0118572 and OCE-9819666.

References

Aharonov, E., J. A. Whitehead, P. B. Kelemen, and M. Spiegelman, Channeling instability of upwelling melt in the mantle, *J. Geophys. Res.*, *100*, 20,433–20,450, 1995.

Allan, J. F., and H. J. B. Dick, Cr-rich spinels as a tracer for melt migration and melt-wall rock interaction in the mantle: Hess Deep, Leg 147, *Ocean Drill. Program Sci. Res.*, *147*, 157–172, 1996.

Arai, S., and K. Matsukage, Petrology of gabbro-troctolite-peridotite complex from Hess Deep, Equatorial Pacific: implications for mantle-melt interaction within the oceanic lithosphere, *Ocean Drill. Program Sci. Res.*, *147*, 135–155, 1996.

Augé, T., Chromite deposits in the northern Oman ophiolite: mineralogical constraints, *Mineral. Deposita*, *22*, 1–10, 1987.

Barton, C. A., and M. D. Zoback, Self-similar distribution and properties of macroscopic fractures at depth in crystalline rock in the Cajon Pass Scientific borehole, *J. Geophys. Res.*, *97*, 5181–5200, 1992.

Beattie, P., Uranium- thorium disequilibria and partitioning on melting of garnet peridotite, *Nature*, *363*, 63–65, 1993.

Boudier, F., and R. G. Coleman, Cross section through the peridotite in the Samail ophiolite, southeastern Oman mountains, *J. Geophys. Res.*, *86*, 2573–2592, 1981.

Brearley, M., and C. M. Scarfe, Dissolution rates of upper mantle minerals in an alkali basalt melt at high pressure: An experimental study and implications for ultramafic xenolith survival, *J. Petrol.*, *27*, 1157–1182, 1986.

Cannat, M., How thick is the magmatic crust at slow spreading oceanic ridges?, *J. Geophys. Res.*, *101*, 2847–2857, 1996.

Cannat, M., G. Ceuleneer, and J. Fletcher, Localization of ductile strain and the magmatic evolution of gabbroic rocks drilled at the mid-Atlantic ridge (23°N), in *Proceedings of the Ocean Drilling Program, Scientific Results*, vol. 53, edited by J. A. Karson, M. Cannat, D. J. Miller, and D. Elthon, pp. 77–98, Ocean Drill. Program, College Station, Tex., 1997.

Crank, J., *The Mathematics of Diffusion*, 414 pp., Oxford Univ. Press, New York, 1975.

Daines, M. J., and D. L. Kohlstedt, Transition from porous to channelized flow due to melt/rock reaction during melt migration, *Geophys. Res. Lett.*, *21*, 145–148, 1994.

Dick, H. J. B., Partial melting in the Josephine Peridotite; I, The effect on mineral composition and its consequence for geobarometry and geothermometry, *Am. J. Sci.*, *277*, 801–832, 1977.

Dick, H. J. B., Abyssal peridotites, very slow spreading ridges, and ocean ridge magmatism, in *Magmatism in the Ocean Basins*, edited by A. D. Saunders and M. J. Norry, pp. 71–105, Geol. Soc. of Am., Boulder, Colo., 1989.

Dick, H. J. B., and T. Bullen, Chromian spinel as a petrogenetic indicator in abyssal and alpine-type peridotites and spatially associated lavas, *Contrib. Mineral. Petrol.*, *86*, 54–76, 1984.

Dick, H. J. B., and J. H. Natland, Late-stage melt evolution and transport in the shallow mantle beneath the East Pacific Rise, in *Proceedings of the Ocean Drilling Program, Scientific Results*, vol. 147, edited by C. Mevel, K. M. Gillis, J. F. Allan, and P. S. Meyer, pp. 103–134, Ocean Drill. Program, College Station, Tex., 1996.

Dunn, R. A., D. R. Toomey, and S. C. Solomon, Three-dimensional seismic structure and physical properties of the crust and shallow mantle beneath the East Pacific Rise at 9°30′N, *J. Geophys. Res.*, *105*, 23,537–23,555, 2000.

Elthon, D., Isomolar and isostructural pseudo-liquidus phase diagrams for oceanic basalts, *Am. Mineral.*, *68*, 506–511, 1983.

Elthon, D., Pressure of origin of primary mid-ocean ridge basalts, in *Magmatism in the Ocean Basins*, edited by A. D. Saunders and M. J. Norry, pp. 125–136, Geol. Soc. of Am., Boulder, Colo., 1989.

Elthon, D., and C. M. Scarfe, High pressure phase equilibria of a high-magnesia basalt: implications for the origin of mid-ocean ridge basalts, *Year Book Carnegie Inst. Washington*, *79*, 277–281, 1980.

Forsyth, D. W., S. C. Webb, L. M. Dorman, and Y. Shen, Phase velocity of Raleigh waves in the MELT experiment of the east pacific rise, *Science*, *280*, 1235–1238, 1998.

Freeze, R. A., and J. A. Cherry, *Groundwater*, 604 pp., Prentice-Hall, Old Tappan, N. J., 1979.

Hart, S. R., Equilibration during mantle melting: A fractal tree model, *Proc. Natl. Acad. Sci. USA*, *90*, 11,914–11,918, 1993.

Hirschmann, M. M., and E. M. Stolper, A possible role for garnet pyroxenite in the origin of the "garnet signature" in MORB, *Contrib. Mineral. Pet.*, *124*, 185–208, 1996.

Hung, S.-H., D. W. Forsyth, and D. R. Toomey, Can a narrow, melt-rich, low-velocity zone of mantle upwelling be hidden beneath the East Pacific Rise? Limits from waveform modeling and the MELT experiment, *J. Geophys. Res.*, *105*, 7945–7960, 2000.

Johnson, K. T. M., H. J. B. Dick, and N. Shimizu, Melting in the oceanic upper mantle: an ion microprobe study of diopsides in abyssal peridotites, *J. Geophys. Res.*, *95*, 2661–2678, 1990.

Jousselin, D., A. Nicolas, and F. Boudier, Detailed mapping of a mantle diapir below a paleo-spreading center in the Oman Ophiolite, *J. Geophys. Res.*, *103*, 18,153–18,170, 1998.

Kelemen, P. B., Reaction between ultramafic rock and fractionating basaltic magma, I, Phase relations, the origin of calc-alkaline magma series, and the formation of discordant dunite, *J. Petrol.*, *31*, 51–98, 1990.

Kelemen, P. B., and H. J. B. Dick, Focused melt flow and localized deformation in the upper mantle: Juxtaposition of

replacive dunite and ductile shear zones, *J. Geophys. Res.*, *100*, 423–438, 1995.

Kelemen, P. B., N. Shimizu, and V. J. M. Salters, Extraction of mid-ocean ridge basalt from the upwelling mantle by focused flow of melt in dunite channels, *Nature*, *375*, 747–753, 1995a.

Kelemen, P. B., J. A. Whitehead, E. Aharonov, and K. A. Jordahl, Experiments on flow focusing in soluble porous media, with applications to melt extraction from the mantle, *J. Geophys. Res.*, *100*, 475–496, 1995b.

Kelemen, P. B., G. Hirth, N. Shimizu, M. Spiegelman, and H. J. B. Dick, A review of melt migration processes in the adiabatically upwelling mantle beneath spreading ridges, *Philos. Trans. R. Soc., London Ser. A*, *355*, 283–318, 1997.

Kelemen, P. B., M. G. Braun, and G. Hirth, Spatial distribution of melt conduits in the mantle beneath oceanic spreading ridges: Observations from the Ingalls and Oman ophiolites, *Geochem. Geophys. Geosyst.*, *1*, Paper number 1999GC000012, 2000. (Available at http://www.g-cubed.org).

Koga, K. T., N. Shimizu, and T. L. Grove, Disequilibrium trace element redistribution during garnet to spinel facies transformation, in *Proceedings of the 7th International Kimberlite Conference*, edited by J. L. Gurney, M. D. Pascoe, and S. H. Pascoe, pp. 444–451, National Book Printers, Cape Town, South Africa, 1998.

Kuo, L.-C., and R. J. Kirkpatrick, Dissolution of mafic minerals and its implications for the ascent velocities of peridotite-bearing basaltic magmas, *J. Geol.*, *93*, 691–700, 1985a.

Kuo, L.-C., and R. J. Kirkpatrick, Kinetics of crystal dissolution in the system diopside-forsterite-silica, *Am. J. Sci.*, *285*, 51–90, 1985b.

Laslett, G. M., Censoring and edge effects in areal and line transect sampling of rock joint traces, *Math. Geol.*, *14*, 125–140, 1982.

Lesher, C. E., R. L. Hervig, and D. Tinker, Self-diffusion of network formers (silicon and oxygen) in naturally occurring basaltic liquid, *Geochim. Cosmochim. Acta*, *60*, 405–413, 1996.

Lippard, S. J., A. W. Shelton, and I. G. Gass, *The Ophiolite of Northern Oman*, 178 pp., Blackwell, Malden, Mass., 1986.

Lundstrom, C. C., J. Gill, Q. Williams, and M. R. Perfit, Mantle melting and basalt extraction by equilibrium porous flow, *Science*, *270*, 1958–1961, 1995.

McKenzie, D., ^{230}Th-^{238}U disequilibrium and the melting processes beneath ridges axes, *Earth Planet. Sci. Lett.*, *72*, 149–157, 1985.

Nicolas, A., A melt extraction model based on structural studies in mantle peridotites, *J. Petrol.*, *27*, 999–1022, 1986.

Nicolas, A., Melt extraction from mantle peridotites: Hydrofracturing and porous flow, with consequences for oceanic ridge activity, in *Magma Transport and Storage*, edited by M. P. Ryan, pp. 1–26, John Wiley, New York, 1990.

Nicolas, A., and F. Boudier, Mapping oceanic ridge segments in Oman ophiolite, *J. Geophys. Res.*, *100*, 6179–6197, 1995.

Nicolas, A., and B. Ildefonse, Flow mechanism and viscosity in basaltic magma chambers, *Geophys. Res. Lett.*, *16*, 2013–2016, 1996.

Nicolas, A., F. Boudier, and B. Ildefonse, Variable crustal thickness in the Oman Ophiolite; implication for oceanic crust, *J. Geophys. Res.*, *101*, 17,941–17,950, 1996.

Nicolas, A., F. Boudier, B. Ildefonse, and E. Ball, Accretion of Oman and United Arab Emirates ophiolite: Discussion of a new structural map, *Mar. Geophys. Res.*, *21*, 147–179, 2000.

O'Hara, M. J., Primary magmas and the origin of basalts, *Scott. J. Geol.*, *1*, 19–40, 1965.

Pallister, J. S., and C. A. Hopson, Samail ophiolite plutonic suite: field relations, phase variation, cryptic variation and layering, and a model of a spreading ridge magma chamber, *J. Geophys. Res.*, *86*, 2593–2644, 1981.

Pallister, J. S., and R. J. Knight, Rare-earth element geochemistry of the Samail ophiolite near Ibra, Oman, *J. Geophys. Res.*, *86*, 2673–2697, 1981.

Pickering, G., J. M. Bull, and D. L. Sanderson, Sampling power-law distributions, *Tectonophysics*, *248*, 1–20, 1995.

Quick, J. E., Petrology and petrogenesis of the Trinity Peridotite, an upper mantle diapir in the eastern Klamath Mountains, northern California, *J. Geophys. Res.*, *86*, 11,837–11,863, 1981.

Salters, V. J. M., and S. R. Hart, The hafnium paradox and the role of garnet in the source of mid-ocean-ridge basalts, *Nature*, *342*, 420–422, 1989.

Spiegelman, M., Geochemical consequences of melt transport in 2-D: The sensitivity of trace elements to mantle dynamics, *Earth Planet. Sci. Lett.*, *139*, 115–132, 1996.

Spiegelman, M., P. B. Kelemen, and E. Aharonov, Causes and consequences of flow organization during melt transport: The reaction infiltration instability, *J. Geophys. Res.*, *106*, 2061–2078, 2001.

Stolper, E., A phase diagram for mid-ocean ridge basalts: Preliminary results and implications for petrogenesis, *Contrib. Mineral. Petrol.*, *74*, 13–27, 1980.

Suhr, G., Melt migration under oceanic ridges: Inferences from reactive transport modeling of upper mantle hosted dunites, *J. Petrol.*, *40*, 575–599, 1999.

Vera, E. E., J. C. Mutter, P. Buhl, A. A. Orcutt, A. J. Harding, M. E. Kappus, R. S. Detrick, and T. M. Brocher, The structure of 0- to 0.2-My-old crust at 9°N on the East Pacific Rise from expanded spread profiles, *J. Geophys. Res.*, *95*, 15,529–15,556, 1990.

von Bargen, N., and H. S. Waff, Permeablilities, interfacial areas and curvatures of partially molten systems: Results of numerical computations of equilibrium microstructures, *J. Geophys. Res.*, *91*, 9261–9276, 1986.

Weisburg, S., *Applied Linear Regression*, 324 pp., John Wiley, New York, 1985.

Zhang, Y., D. Walker, and C. E. Lesher, Diffusive crystal dissolution, *Contrib. Mineral. Petrol.*, *102*, 492–513, 1989.